Exciton wave function properties probed by diamagnetic shift in disordered quantum wells

M. Grochol,* F. Grosse, and R. Zimmermann
Institut für Physik der Humboldt-Universität zu Berlin, Newtonstrasse 15, 12489 Berlin, Germany
(Received 30 November 2004; published 31 March 2005)

Absorption spectra and wave functions of optically active exciton states in disordered quantum wells are calculated. The interplay between the relative and center-of-mass part of the total exciton wave function is investigated using a perpendicular magnetic field. The diamagnetic shift varies strongly in correspondence with the wave function localization. The full solution reveals failures of the simple factorization in relative and center-of-mass coordinates even for weak global disorder.

DOI: 10.1103/PhysRevB.71.125339 PACS number(s): 78.20.Bh, 78.67.De, 71.35.Cc, 74.35.Ji

I. INTRODUCTION

Semiconductor quantum structures have been a subject of intensive study for many years. Their unique properties enable applications in communication and information technology. However, reduction in size of active layers in these structures leads to strong influence of imperfections. They cannot be avoided even with state-of-the-art growth techniques.

Excitons determine the near band-edge optical properties in semiconductors. Their binding energy grows with quantum confinement (decreasing dimensionality). The sensitivity of the excitonic properties to disorder gives us the possibility to investigate the underlying structure, e.g., in the case of quantum wells the dominant interface and alloy disorder. Experimentally, its influence on excitons was studied by methods enabling high spatial and spectral resolution such as microphotoluminescence,[1–3] scanning near-field optical spectroscopy,[4] and cathodoluminescence.[5] The exciton localization was observed in effective quantum dots formed due to interface disorder.

Theoretically, the disorder effect on excitons in quantum wells was investigated using potentials obtained on the basis of simple growth simulations.[6] The approximation using an undisturbed exciton relative motion in a simple factorization ansatz for the total wave function (WF) was tested. A good agreement for a single absorption spectrum was found. The WF properties were not compared. Within this simple factorization scheme, the statistics of the oscillator strength was studied with two distinct regimes where Anderson localized states or Lifshitz tail states are dominant.[7] Also quantum mechanical level repulsion was demonstrated, revealing good agreement between theory and experiment.[8]

The influence of a perpendicular magnetic field on the exciton in *ideal* quantum structures has gained theoretical interest recently. The exciton diamagnetic shift was calculated in idealized quantum structures.[9] It has been shown to give additional information about the interplay between Coulomb interaction and transversal confinement. The influence of a perpendicular magnetic field on the dispersion relation of the exciton was investigated, too: The transition from a hydrogenlike exciton towards the magnetoexciton [with increased electron-hole separation proportional to center-of-mass (c.m.) momentum and $1/B$] was predicted leading to the increase of the total mass of the exciton.[10]

Furthermore, the combined effect of a perpendicular magnetic field and alloy disorder was also of interest. The shift of the maximum of the photoluminescence (PL) peak towards higher energies was calculated together with a modification of the line shape. The calculation was based on the factorization scheme, but c.m. WF's were treated phenomenologically.[11] The spectroscopic methods with high spectral and spatial resolution enable to follow localized states with magnetic field: As demonstrated in the well-known near-field optical experiment by Hess *et al.*[4] and recently in microphotoluminescence spectra[12] on GaAlAs/GaAs quantum wells the diamagnetic shift differs between localized excitons. Even negative diamagnetic shifts or spin splitted triplets were observed. The spin splitted doublets were taken as evidence of localized excitons.[4] Also recent PL measurements reveal interesting features with magnetic field, namely the change of the PL peak shape and shift of the maximum.[13] The calculation explaining the experimental observations was performed with a rather simplified theory assuming a complete localization of holes in the GaAsSbN/GaAs structure under study.

In this paper a theory for excitons in disordered quantum wells under application of a perpendicular magnetic field is developed. Special emphasis is given to single localized exciton states. The relation between the energetic shift and localization is investigated by a numerical solution without factorizing the exciton relative and c.m. motion. The quality of a factorized ansatz is discussed. The paper is organized as follows. The theoretical treatment is explained in Sec. II. In Sec. III, first, the results of the simple factorization approach and the full solution are compared for uncorrelated disorder. Second, the correlation between the WF properties and the diamagnetic shift is investigated. The conclusions are followed by an appendix describing numerical details.

II. THEORY

The exciton in a disordered quantum well is described within the envelope function formalism[6] applying the effective mass approximation. Including a perpendicular magnetic field the Hamiltonian takes the following form:

$$\hat{H} = \sum_{a=e,h} \left(\frac{1}{2m_{a,\|}} (\hat{\mathbf{p}}_a - e\mathbf{A}_a)^2 + \frac{1}{2m_{a,\perp}} \hat{p}_{z_a}^2 + U_a(z_a) + W_a(\mathbf{r}_a, z_a) \right) - \frac{e^2}{4\pi\epsilon_0\epsilon\sqrt{(\mathbf{r}_e - \mathbf{r}_h)^2 + (z_e - z_h)^2}}, \quad (1)$$

where "a" denotes either electron (e) or hole (h), $m_{a,\|}$ ($m_{a,\perp}$) is the in-plane (growth direction) carrier effective mass ($\|$ is dropped in the following), $U_a(z_a)$ is the confinement potential in the growth direction, $W_a(\mathbf{r}_a, z_a)$ is the disorder potential, ϵ is the static dielectric constant of the well material, and $\mathbf{r}_a$ denotes in-plane coordinates while z_a is the coordinate in the growth direction. A Coulomb gauge in relative coordinates for the magnetic field is chosen

$$\mathbf{A}_e = \frac{B}{2}[y_e - y_h, -(x_e - x_h), 0], \quad \mathbf{A}_h = -\mathbf{A}_e. \quad (2)$$

This gauge induces oscillating terms in the WF of type $\exp[-ie\mathbf{A}(\mathbf{r})\cdot\mathbf{r}/\hbar]$, but these are restricted to the WF extension in relative space, which is of the order of the exciton Bohr radius. Other gauges with a dependence of the vector potential on the c.m. coordinates would lead to oscillating features across the entire sample, which is not suitable for a numerical solution using a finite grid size.

The spin degrees of freedom would contribute a term linear in magnetic field (neglecting spin-orbit coupling)[14]

$$\hat{H}^{spin} = \sum_{a=e,h} g_a^* \mu_B B \sigma_a^z, \quad (3)$$

where g_a^* are effective g factors for electron and hole, μ_B is the Bohr magneton, and σ^z is the Pauli spin matrix. In the excitonic case the total angular momentum $J = L + \sigma$ of the Bloch function has to be considered in the first approximation (L is the orbital angular momentum). Only excitons with $J = \pm 1$ are optically active. Since electron and hole have different g factors, the spin term does not vanish for the exciton Hamiltonian.[15] By neglecting the spin dependent part (Zeeman splitting) our theory applies therefore for the average of the spin splitted energies.

Assuming narrow quantum wells, a separation of the WF for in-plane and growth direction is taken (single sublevel approximation),

$$\Phi_\alpha(\mathbf{r}_e, \mathbf{r}_h, z_e, z_h; B) = \Psi_\alpha(\mathbf{r}, \mathbf{R}; B) u_e(z_e) u_h(z_h), \quad (4)$$

where $u_a(z_a)$ are confinement WF's. Relative $\mathbf{r} = \mathbf{r}_e - \mathbf{r}_h$ and c.m. coordinates $\mathbf{R} = (m_e\mathbf{r}_e + m_h\mathbf{r}_h)/M$ with total exciton mass $M = m_e + m_h$ and reduced exciton mass $\mu = m_e m_h / M$ were introduced. The Hamiltonian can be rewritten in the following way:

$$\hat{H}_{exc} = -\frac{\hbar^2}{2\mu}\Delta_{\mathbf{r}} - \frac{\hbar^2}{2M}\Delta_{\mathbf{R}} + \frac{e^2B^2}{8\mu}r^2 + \frac{eB}{2}\left(\frac{1}{m_e} - \frac{1}{m_h}\right) \times i\hbar(y\partial_x - x\partial_y) + \frac{eB}{M} i\hbar(y\partial_X - x\partial_Y) + V_e\left(\mathbf{R} + \frac{m_h}{M}\mathbf{r}\right) + V_h\left(\mathbf{R} - \frac{m_e}{M}\mathbf{r}\right) - V_C(r), \quad (5)$$

where V_C is the averaged Coulomb potential

$$V_C(\mathbf{r}) = \int dz_e dz_h u_e^2(z_e) u_h^2(z_h) \frac{e^2}{4\pi\epsilon_0\epsilon\sqrt{\mathbf{r}^2 + (z_e - z_h)^2}}, \quad (6)$$

and $V_a(\mathbf{r}_a)$ is the in-plane disorder, which is in detail described in the Appendix. The eigenenergies are solutions of the stationary Schrödinger equation

$$\hat{H}_{exc}\Psi_\alpha(\mathbf{r}, \mathbf{R}; B) = E_\alpha(B)\Psi_\alpha(\mathbf{r}, \mathbf{R}; B), \quad (7)$$

at a given magnetic field B. Zero of energy is taken at the quantum well gap plus electron and hole confinement energy.

In the Hamiltonian Eq. (5) there are three magnetic field dependent terms: The first one ($\sim B^2$) gives rise to the well-known quadratic diamagnetic shift. This term gives always a positive contribution to the energy. The second term ($\sim B$) is proportional to the angular momentum in the growth direction. Without disorder, this term is zero for optically active states (s states). The last term describes the B dependent mixing of relative and c.m. motion. The second and the third term together contribute negatively to the ground state energy for small magnetic fields, which follows simply from first and second order perturbation theory.

For our purposes a state dependent *diamagnetic shift* Δ_α is defined

$$\Delta_\alpha(B) = E_\alpha(B) - E_\alpha(0). \quad (8)$$

The numerical treatment, which is described in detail in the appendix, is equivalent to compute the eigenenergies $E_\alpha(B)$ and the oscillator strengths $M_\alpha(B)$

$$M_\alpha(B) = \frac{1}{\Omega}\int d\mathbf{R}\Psi_\alpha(\mathbf{0}, \mathbf{R}; B), \quad (9)$$

which allows us to construct the optical density (or absorption) as

$$D(\omega; B) = \sum_\alpha \pi M_\alpha^2(B)\delta(\hbar\omega - E_\alpha(B)). \quad (10)$$

Our calculations are performed for a 4 nm wide GaAs quantum well embedded in $Ga_{0.7}Al_{0.3}As$ barriers with 65% band offset for electrons. GaAs material parameters have been taken as $m_{h,\perp} = (0.3774 + 0.1053x)m_0$, $m_{e,\perp} = (0.06657 + 0.0575x)m_0$ (x stands for Al concentration), $m_{h,\|} = 0.233m_0$,[16] $m_{e,\|} = 0.06657m_0$, $\epsilon = 12.5$. Electron and hole confinement energies add up to 128.2 meV.

A. Simple factorization

Here the standard simple factorization ansatz is briefly described. For weak disorder an unperturbed relative motion

(state independent, exact for no-disorder) can be assumed, thus factorizing the total WF into relative and c.m. part[6]

$$\Psi_\alpha(\mathbf{r},\mathbf{R};B) = \phi_{1s}(\mathbf{r};B)\psi_\alpha(\mathbf{R};B), \tag{11}$$

where $\phi_{1s}(\mathbf{r};B)$ is the solution of the relative motion Schrödinger equation without disorder,

$$\left(-\frac{\hbar^2}{2\mu}\Delta_\mathbf{r} + \frac{e^2B^2}{8\mu}r^2 - V_C(r) - E_{1s}(B)\right)\phi_{1s}(\mathbf{r};B) = 0. \tag{12}$$

As mentioned before, the term linear in B is zero for s states. Proceeding further,[6] the c.m. equation reads

$$\left(-\frac{\hbar^2}{2M}\Delta_\mathbf{R} + V(\mathbf{R};B)\right)\psi_\alpha(\mathbf{R};B) = E_\alpha(B)\psi_\alpha(\mathbf{R};B) \tag{13}$$

with the disorder potential averaged by the relative WF

$$V(\mathbf{R};B) = \sum_{a=e,h}\int d\mathbf{r}_a\beta_a^2\phi_{1s}^2[\beta_a(\mathbf{r}_a - \mathbf{R});B]V_a(\mathbf{r}_a), \tag{14}$$

where $\beta_e = M/m_h$ and $\beta_h = M/m_e$. Within the factorization ansatz the oscillator strength Eq. (9) reduces to

$$M_\alpha^{fact}(B) = \frac{1}{\Omega}\phi_{1s}(0;B)\int d\mathbf{R}\psi_\alpha(\mathbf{R};B). \tag{15}$$

The state dependent diamagnetic shift Eq. (8) takes the following form:

$$\Delta_\alpha(B) = E_{1s}(B) - E_{1s}(0) + E_\alpha(B) - E_\alpha(0). \tag{16}$$

The first part $E_{1s}(B) - E_{1s}(0)$ is state independent and proportional to B^2 for small B. The second part $E_\alpha(B) - E_\alpha(0)$ is state dependent and also proportional to B^2 for small B. Since B tends to shrink the WF $\phi_{1s}(\mathbf{r};B)$, averaging is less effective: Potential minima become deeper, and have greater curvature. The c.m. potential change is quadratic for small B as can be easily checked by inserting a WF from the second order perturbation theory ($\sim B^2$) into Eq. (14).

B. Analysis of the WF

The complicated behavior of the four coordinate WF can be better investigated by focusing on the projections of the WF,

$$\phi_\alpha^2(\mathbf{r};B) = \int d\mathbf{R}\Psi_\alpha^2(\mathbf{r},\mathbf{R};B), \tag{17}$$

$$\psi_\alpha^2(\mathbf{R};B) = \int d\mathbf{r}\Psi_\alpha^2(\mathbf{r},\mathbf{R};B). \tag{18}$$

The projected relative WF $\phi_\alpha^2(\mathbf{r};B)$ does not vary much qualitatively between different local ground states: It is nodeless and rather isotropic due to the strength of the Coulomb interaction. Therefore, the value $\phi_\alpha^2(\mathbf{0};B)$ is sufficient to characterize $\phi_\alpha^2(\mathbf{r};B)$ and gives information about the extension of the relative WF. We define a relative measure related to the no-disorder and zero B field case by

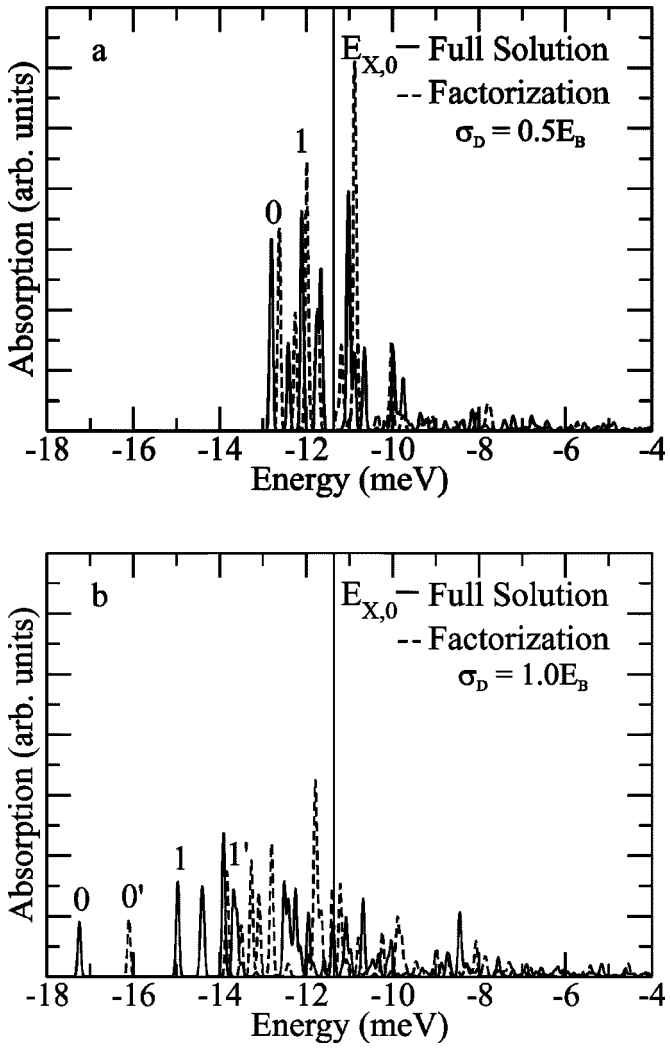

FIG. 1. Calculated absorption spectra for two different strengths of the disorder [$\sigma_D = 0.5\ E_B$ (a) and $\sigma_D = 1.0\ E_B$ (b)]. The full solution (solid) and factorization (dashed) are plotted. Two optically active states for each calculation are marked [with $0'$, $1'$ for factorization in (b)]. Corresponding wave functions are shown in Fig. 2.

$$\rho_\alpha = \frac{\phi_\alpha^2(\mathbf{0};B)}{\phi_{1s}^2(\mathbf{0};0)}, \tag{19}$$

where $\phi_{1s}^2(\mathbf{0};0) = 0.00582\ \mathrm{nm}^{-2}$. The larger the value ρ_α, the smaller is the relative projection extension Eq. (17). The c.m. projections Eq. (18) are plotted using contour plots with 6 lines between maximum and minimum of each WF. The localization of the WF can be visualized in this way.

III. RESULTS AND DISCUSSION

A. Comparison between full solution and factorization

1. No magnetic field

Absorption spectra calculated with and without factorization are compared for a single disorder realization in Fig. 1. Good agreement is expected in the case of weak disorder where the factorization assumption of unperturbed relative

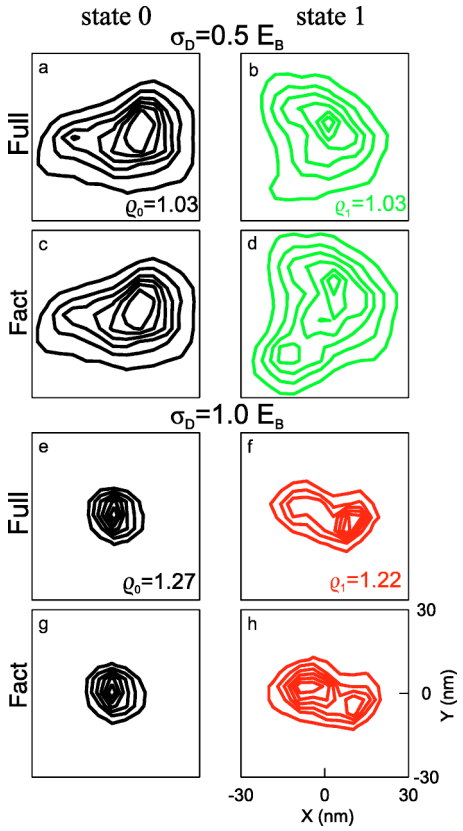

FIG. 2. (Color online) The probability densities of the c.m. part (projection) of the total wave functions Eq. (18) calculated for states (0, 1) of Fig. 1 as contour plots (Ref. 17). Full solution [(a), (b), (e), (f)] and factorization [(c), (d), (g), (h)] for $\sigma_D=0.5\ E_B$ (a)–(d) and $\sigma_D=1.0\ E_B$ (e)–(h). The values ρ_α Eq. (19) are shown for each wave function in the full solution (in the factorization $\rho_\alpha \equiv 1.00$ per definition). Total simulation size is 160×160 nm^2 with a grid step of 4 nm.

motion is almost valid. Indeed, this is found in Fig. 1(a), *seemingly* approving the factorization. However, the ground state energy in the full solution is lower than in the factorization, which is consistent with variational arguments.The different effective (numerical) averaging in the full solution and factorization also contributes to the 0.2 meV rigid shift of all states in Fig. 1(a). Our calculations have shown that these shifts are magnetic field independent. The spectrum agreement worsens above the ideal exciton position $E_{X,0}$ (line in Fig. 1: $E_{X,0}=-E_B=-11.4$ meV) where states mix with the ideal 2*s* state. Due to orthogonality, these states are modified by different local ground states, even if their relative parts in the full solution and factorization were similar. In the case of stronger disorder [Fig. 1(b)] even the qualitative agreement is lost. A correspondence between WF's may be expected only for the first few tail states since they are local ground states in deep minima.

For a better understanding it is important to distinguish between the local potential shape relevant for the localized exciton state and the global disorder given by the variation σ_D. The local potential is characterized by a limited number of parameters, e.g., discrete values on grid points close to the position of the localized exciton. The change of the (global) disorder strength modifies the potential statistics. A relatively shallow minimum, which is highly probable in case of weak disorder, is less likely in a case with stronger disorder, where more deeper minima with strong curvatures exist. The disorder strength determines *only the probability* of highly localized states which are not well described by a simple factorization ansatz since the effective compression of the relative part is neglected. The stronger the global disorder, the higher the probability that the factorization fails.

Next, we concentrate on the WF properties. The c.m. projection Eq. (18) and the relative WF measure ρ_α are shown in Fig. 2 for the same disorder realization used in Fig. 1. Several interesting features turn up. The values of ρ_α vary in the full solution between states: The most localized c.m. states have also the most compressed relative parts (greatest values ρ_α). This is physically understandable since a stronger localization of electron and hole leads to an effectively stronger Coulomb interaction, which is then state dependent.

Another appealing feature is the (dis)agreement of c.m. parts in the full solution and the factorization. The projections Eq. (17) and Eq. (18) play a different role: The relative part averages the disorder potential for the c.m. motion. This means that a small alteration in the relative part leads to a small alteration in the effective c.m. disorder potential and further in the c.m. localization (Fig. 2). This simple picture is not valid in the case of stronger disorder [Fig. 1(b)]. The ideal relative WF $\phi_{1s}(\mathbf{r};B)$ averages so that some minima can become too shallow (or even disappear), since $\phi_{1s}(\mathbf{r};B)$ is more extended in size compared with the full solution. The energetic position can be shifted and the c.m. WF can be changed [see specifically Figs. 2(f) and 2(h)].

Using the WF projections Eq. (17) and Eq. (18) we compare the localization of the c.m. projection in Fig. 2 and the oscillator strength of these states plotted in Fig. 1. The correspondence is found for the two plotted states: the most localized c.m. projection has the smallest oscillator strength. The contribution of the relative projection grows with the compression unlike the c.m. contribution which decreases with localization. This implies that the oscillator strength is predominantly determined by c.m. localization for local ground states.[18]

2. Magnetic field

So far only the disorder effect on the exciton was discussed. Now we include the perpendicular magnetic field in our comparison between the full solution and the factorization.

We focus again on the WF projections Eq. (17) and Eq. (18) for a deeper understanding: The relative projection is affected proportional to its extension ($\sim\langle r^2\rangle$). Since in the factorization the ideal relative WF $\phi_{1s}(\mathbf{r};B)$ is used, it changes more with magnetic field than in the full solution, which is already shrunk due to localization as discussed above. This is schematically depicted in Figs. 3(a) and 3(b). The effective averaged c.m. potential minimum is then more shallow in the factorization, and the bound state has a higher energy [Figs. 3(c) and 3(d)]. The magnetic field has a greater impact on the effective c.m. potential in the factorization [Fig. 3(e)] than in the full solution [Fig. 3(f)]. In the factor-

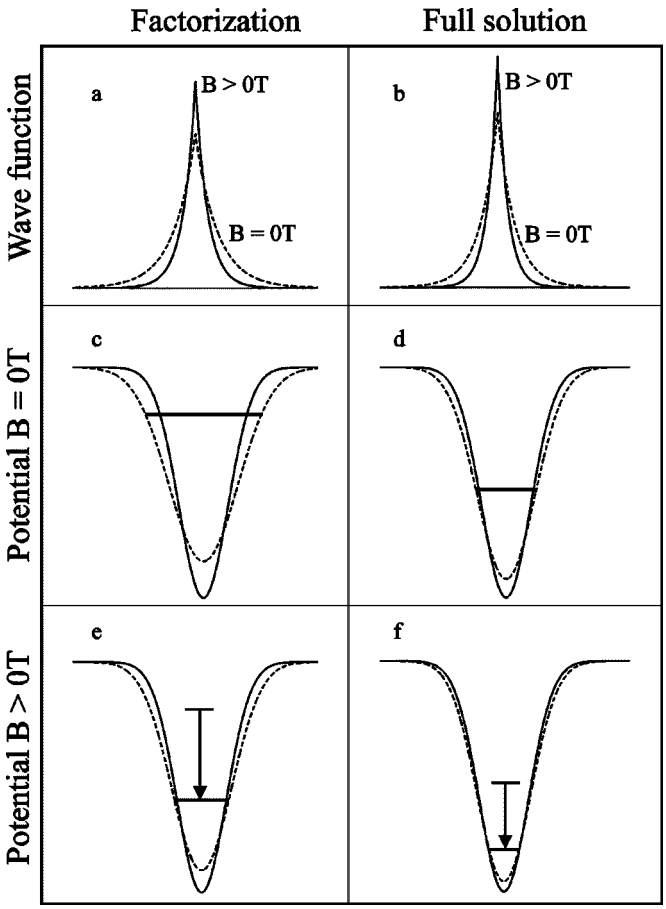

FIG. 3. Schematic drawing of the exciton relative wave function [factorization (a) and full solution (b)] and original (solid) and averaged potential (dashed) as a functions of magnetic field. Energy levels are also depicted. The arrows indicate the negative c.m. contribution to the diamagnetic shift; the positive contribution from the relative motion is not shown.

ization both contributions to the diamagnetic shift are overestimated: The relative one proportional to $\langle r^2 \rangle$ (not shown in Fig. 3) and the downshift of the c.m. energy. If full solution and factorization agree without magnetic field, then also the diamagnetic shift agrees. In other cases (depending on local disorder), agreement is not to be expected. Unfortunately, looking at the potential landscape it is not clear from the beginning, to which extent the factorization and the full solution agree.

B. Full solution: Localization and magnetic field

The change of the absorption spectra with magnetic field is shown in Fig. 4. The first few localized states can be recognized unambiguously, and the diamagnetic shift can be read off easily from Fig. 4(a). The changes of the oscillator strength $M_\alpha(B)$ with magnetic field can be extracted, too, but are marginal. The effects of the magnetic field on averaged (over several disorder realizations) spectra [Fig. 4(b)] are the shift of the maximum and a widening since the diamagnetic shift $\Delta_\alpha(B)$ increases in average with energy $E_\alpha(0)$. This average increase can also explain the changes in PL spectra.

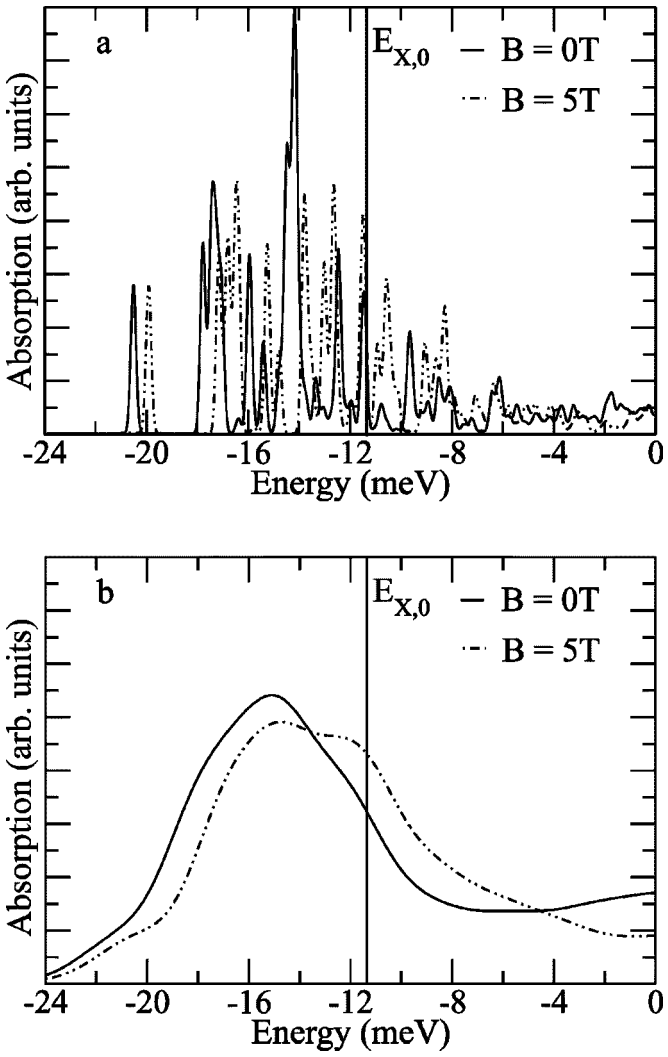

FIG. 4. Absorption spectra calculated for two different magnetic fields (solid 0 T, dashed 5 T) and for a single disorder realization (a) (Gauss broadening of single line σ=0.1 meV) and averaged over 12 realizations of disorder (b) (Gauss broadening of single line σ=1.0 meV). Disorder strength in both cases σ_D=1.5 E_B.

Here, the occupation of states enters in addition. Since higher states have lower occupation, the effect is weaker with respect to absorption spectra. Our simulations predict the widening with magnetic field in accordance with experiment.[13]

The influence of the magnetic field on the WF's can be seen in Fig. 5. The correlation between c.m. and relative projection is observed again. A new feature is the correlation between the diamagnetic shift and WF extension. The diamagnetic shift for the three states is given in Fig. 5(b). As mentioned above the relative part is affected proportionally to its extension ($\langle r^2 \rangle$), which is illustrated by the change of ρ_α values in Fig. 5, where the smallest change with magnetic field is found for the ground state. In general, the diamagnetic shift Δ_α is inversely correlated to the relative measure ρ_α. The positive relative contribution $\sim\langle r^2 \rangle$ is dominant. The c.m. contribution is negative but not necessarily small in absolute value. Minor modifications of the relative part may induce substantial modifications of the c.m. energy.

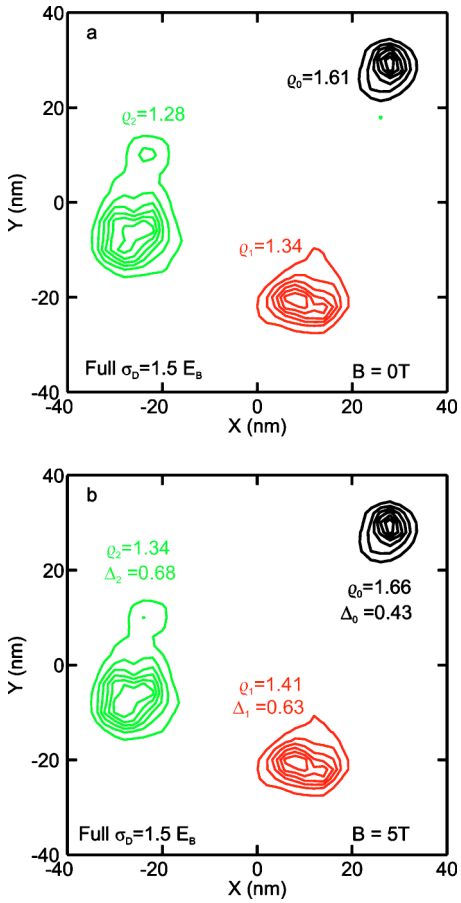

FIG. 5. (Color online) The probability densities of the center-of-mass projection of the total wave functions Eq. (18) calculated for the energetically lowest three states of the full solution for $\sigma_D = 1.5\ E_B$ [(a) $B=0$ T, (b) $B=5$ T] as contour plots (Ref. 17). A grid step of $\Delta = 2$ nm is used. The values ρ_α Eq. (19) are shown for each wave function. The diamagnetic shift $\Delta_\alpha(B)$ in meV is given, also (without disorder, $\rho_{1s}=1.123$ and $\Delta_{1s}=1.08$ meV).

Taking calculations for different realizations and disorder strengths, a statistics of the diamagnetic shift can be obtained as shown in Fig. 6. The analysis is always performed only for the first few tail states. The increase of the average diamagnetic shift with eigenenergy is obvious. The no-disorder case is marked as a star, and is properly positioned on the trend line. The existence of the trend line for the diamagnetic shift going through several disorder strengths is nontrivial. In the present case, value and shape of minima are mainly fixed by the eigenenergy and depend much less on the global disorder strength.

Finally, we shortly comment on the differences between the full solution and the factorization regarding the diamagnetic shift. The deviations increase with decreasing eigenenergy. This is well understood since highly localized states are not properly described in the factorization. The state independent relative WF in the factorization may even lead to negative diamagnetic shifts in very deep potential minima, which is never observed in the full solution. Experimentally, negative diamagnetic shifts have been observed only exceptionally.[4] In theory, the basic question arises: Can the diamagnetic shift be negative at all? We have not found a rigorous answer yet.

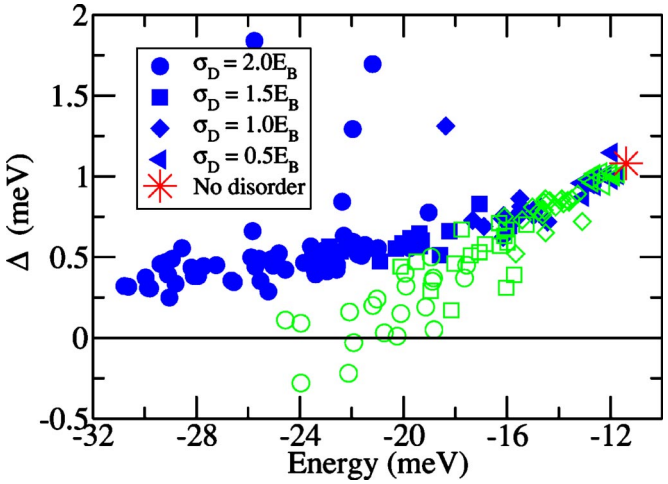

FIG. 6. (Color online) The distribution of the diamagnetic shifts at $B=5$ T calculated with the full solution (full symbols) and factorization (open symbols) for different strengths of disorder.

IV. CONCLUSIONS AND OUTLOOK

Exciton states in disordered quantum wells under the presence of a perpendicular magnetic field are studied. The WF behavior is discussed in detail: The relative part of the WF is state dependent and shrunk in contrast to the state independent picture in the factorization scheme. This shrinkage leads in turn to a more localized c.m. part. Therefore, the correct description of the diamagnetic shift requires to go beyond the simple factorization ansatz.

The diamagnetic shift varies strongly among different localized states but a general trend exists. The WF properties are determined by the local potential only. The most localized states show the smallest diamagnetic shift. This correlation allows an experimental investigation of the statistics of the WF localization.

From the application side a very important question evolves: Is it possible to reconstruct local potential properties from the diamagnetic shift? The correlation between the diamagnetic shift and localization could be a way to access information about the local potential landscape and therefore the underlying quantum structure. A clear statement makes additional investigations necessary, particularly with respect to long range potential correlations.

ACKNOWLEDGMENTS

We acknowledge support from the DFG Graduiertenkolleg 1025: "Grundlagen und Funktionalität von größen- und grenzflächenbestimmten Materialien: Spin- und Optoelektronik" and discussions with C. Ropers.

APPENDIX: NUMERICS

1. Method

The linear optical susceptibility[19] in the frequency domain is considered at first

$$\chi(\omega) = \langle\mu|[\hat{H} - \hbar\omega + i0]^{-1}|\mu\rangle, \tag{A1}$$

$$\langle r|\mu\rangle = \frac{d_{cv}}{\Omega}\delta(\mathbf{r}_e - \mathbf{r}_h), \tag{A2}$$

where $|\mu\rangle$ represents an electron-hole excitation state from the semiconductor vacuum with interband dipole matrix element d_{cv} and the simulation area Ω. The optical density $D(\omega)$ Eq. (10) is defined as the imaginary part of the susceptibility

$$D(\omega) = \mathrm{Im}\,\chi(\omega). \tag{A3}$$

The efficient calculation of the eigenvalues and eigenfunctions of the full electron-hole Hamiltonian Eq. (5) goes beyond the capability of any direct eigenvalue solver, even if only the first few eigenstates are needed: Our standard calculation is performed for 30 or 40 grid points for every coordinate, which gives in total $N=30^4=810.000$ or $N=40^4=2.560.000$ points (N being the matrix dimension). Instead the susceptibility can be calculated using the time evolution of the wave function

$$i\hbar\frac{d}{dt}|\Psi(t)\rangle = \hat{H}|\Psi(t)\rangle, \quad |\Psi(0)\rangle = |\mu\rangle, \tag{A4}$$

and performing the Fourier transformation with the projection of the wave function $|\Psi(t)\rangle$ onto $|\mu\rangle$

$$\chi(\omega) = \frac{i}{\hbar}\int_0^\infty dt e^{-i\omega t}\langle\Psi(t)|\mu\rangle. \tag{A5}$$

The quick and efficient implementation of the time evolution Eq. (A4) by the Leapfrog method proposed in Ref. 20 was adopted. In order to handle the effects of finite time integration in the Fourier transformation a small Gauss damping is introduced[21]

$$D(\omega) = \mathrm{Re}\frac{1}{\hbar}\int_0^\infty dt e^{-i\omega t}e^{-(\sigma t/\hbar)^2}\langle\Psi(t)|\mu\rangle. \tag{A6}$$

The expansion of $|\Psi(t)\rangle$ into the eigenfunctions $|\Psi_\alpha\rangle$ of the Hamiltonian Eq. (5)

$$|\Psi(t)\rangle = \sum_\alpha |\Psi_\alpha\rangle\langle\Psi_\alpha|\mu\rangle e^{-iE_\alpha t/\hbar}, \tag{A7}$$

$$\hat{H}_{exc}|\Psi_\alpha\rangle = E_\alpha|\Psi_\alpha\rangle \tag{A8}$$

gives a Gauss broadened optical density Eq. (10)

$$D(\omega) = \sum_\alpha \pi|M_\alpha|^2\frac{1}{\sqrt{2\pi}\sigma}\exp\left(-\frac{(\hbar\omega - E_\alpha)^2}{2\sigma^2}\right),$$

$$M_\alpha = \langle\Psi_\alpha|\mu\rangle. \tag{A9}$$

Given the eigenenergy, the corresponding eigenfunction can be extracted integrating over the time dependent WF in a second run

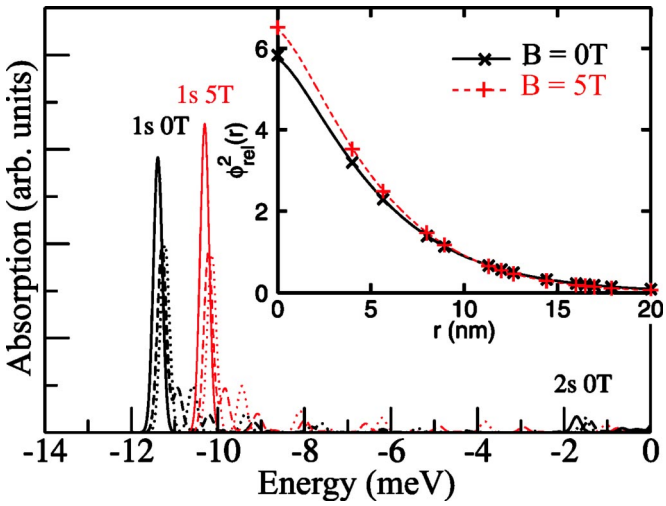

FIG. 7. (Color online) Absorption spectra without disorder calculated using the exact solution taking Eq. (12) for all states (solid). For the full solution, two simulation sizes are used: $N=30^4$ (dotted) and $N=40^4$ (dashed) with a grid step of 4 nm. Inset: The probability densities of the relative part of the total wave function Eq. (18) calculated for the 1*s* state of the full solution (crosses) and calculated exactly (line) for 0 T and 5 T (units in 10^{-3} nm^{-2}).

$$\langle\mathbf{r},\mathbf{R}|\Psi_\alpha\rangle \sim \int dt\langle\mathbf{r},\mathbf{R}|\Psi(t)\rangle e^{iE_\alpha t/\hbar}e^{-(\sigma t/\hbar)^2}. \tag{A10}$$

In this way, however, only WF's of energetically well separated eigenstates can be obtained.

2. Implementation and tests

The electron and hole confinement WF's $u_a(z_a)$ Eq. (4) without disorder are calculated numerically. Then, the Coulomb averaging Eq. (6) is performed and the factorized Schrödinger equation (12) is numerically solved.[21] The WF $\phi_{1s}(\mathbf{r};B)$ obtained in this way is used twice: in the factorization approach and to generate the discretized Coulomb potential for the full solution using the identity

$$V_C(r) = \frac{\left(\frac{\hbar^2}{2\mu}\Delta_\mathbf{r}\right)\phi_{1s}(\mathbf{r};0)}{\phi_{1s}(\mathbf{r};0)} + E_{1s}(0), \tag{A11}$$

as introduced by Glutsch *et al.*[20] This method also handles the Coulomb singularity at the origin. Two values of the grid step were used: 4 nm and 2 nm. The Hamiltonian Eq. (5) in electron and hole coordinates is given by

$$\hat{H}_{exc} = -\frac{\hbar^2}{2m_e}\Delta_{\mathbf{r}_e} - \frac{\hbar^2}{2m_h}\Delta_{\mathbf{r}_h} + \frac{e^2B^2}{8\mu}(\mathbf{r}_e - \mathbf{r}_h)^2 + V_e(\mathbf{r}_e) + V_h(\mathbf{r}_h)$$
$$- V_C(r) + \frac{eB}{2m_e}i\hbar[(y_e - y_h)\partial_{x_e} - (x_e - x_h)\partial_{y_e}]$$
$$+ \frac{eB}{2m_h}i\hbar[(y_e - y_h)\partial_{x_h} - (x_e - x_h)\partial_{y_h}], \tag{A12}$$

which is implemented instead of Eq. (5). The choice of elec-

tron and hole coordinates is advantageous for a possible inclusion of disorder from growth simulations.[6]

The factorization ansatz Eq. (11) holds precisely in the no-disorder case, which is used to test the full solution. The only optically active state has a constant c.m. part (delocalized). The absorption spectra plotted in Fig. 7 full and exact solution. Due to a combined effect of boundary conditions and finite simulation size, the exact spectrum is not fully reconstructed in the full solution. There is a small energy shift of the dominant peak and additional small peaks appear. Increasing the simulation size the satellite peaks move towards the main peak.

In the presence of disorder the c.m. projection of the WF is localized and far less sensitive to the boundary conditions. Therefore, our implementation is suited for the disorder case (localized states).

An important feature is the almost correct reconstruction in the full solution of the 2*s* exciton state [the second eigenvalue E_{2s} of Eq. (12) with eigenfunction $\phi_{2s}(\mathbf{r})$] since the potential is constructed only with the 1*s* WF. The diamagnetic shifts of the 1*s* and 2*s* excitons are also obtained correctly with less than 3% error. The relative parts of WF's plotted in the inset of Fig. 7 demonstrate the good agreement as well.

3. Disorder potential

No explicit averaging of an underlying atomistic disorder by confinement WF's (Ref. 6) is carried out. Instead Gaussian distributed and spatially uncorrelated fluctuations of the gap V are generated, thus neglecting long range correlations:

$$\langle V_i \rangle = 0, \quad \langle V_i V_j \rangle = \delta_{ij} \sigma_D^2, \tag{A13}$$

$$V_{e,i} = 0.65 V_i, \quad V_{h,i} = 0.35 V_i, \tag{A14}$$

where V_i is a potential value on the ith point of the two dimensional grid. Electron and hole disorder is fully correlated on the same site since it depends on the same local quantum well width. We use here the same band offsets as for the quantum well potential barrier. Doing so, we neglect the (mass dependent) averaging by the confinement wave functions.[6] This would lead to minor changes in the band offsets (0.72 electron) and consequently in the results.

*Electronic address: michal.grochol@physik.hu-berlin.de; URL: http://www-semic.physik.hu-berlin.de

[1] A. Zrenner, L. V. Butov, M. Hagn, G. Abstreiter, G. Böhm, and G. Weimann, Phys. Rev. Lett. **72**, 3382 (1994).
[2] K. Brunner, G. Abstreiter, G. Böhm, G. Tränkle, and G. Weimann, Phys. Rev. Lett. **73**, 1138 (1994).
[3] D. Gammon, E. S. Snow, and D. S. Katzer, Appl. Phys. Lett. **67**, 2391 (1995).
[4] H. F. Hess, E. Betzig, T. D. Harris, L. N. Pfeiffer, and K. W. West, Science **264**, 1740 (1994).
[5] E. Runge, J. Menniger, U. Jahn, R. Hey, and H. T. Grahn, Phys. Rev. B **52**, 12 207 (1995).
[6] R. Zimmermann, R. Grosse, and E. Runge, Pure Appl. Chem. **69**, 1179 (1997).
[7] E. Runge and R. Zimmermann, Phys. Status Solidi B **221**, 269 (2000).
[8] F. Intonti, V. Emiliani, C. Lienau, T. Elsaesser, V. Savona, E. Runge, R. Zimmermann, R. Nötzel, and K. H. Ploog, Phys. Rev. Lett. **87**, 076801 (2001).
[9] S. N. Walck and T. L. Reinecke, Phys. Rev. B **57**, 9088 (1998).
[10] Y. E. Lozovik, I. V. Ovchinnikov, S. Y. Volkov, L. V. Butov, and D. S. Chemla, Phys. Rev. B **65**, 235304 (2002).
[11] S. K. Lyo, Phys. Rev. B **48**, 2152 (1994).
[12] C. Ropers, Master thesis, Göttingen, 2003.
[13] R. T. Senger, K. K. Bajaj, E. D. Jones, N. A. Modine, K. E. Waldrip, F. Jalali, J. F. Klem, G. M. Peake, X. Wei, and S. W. Tozer, Appl. Phys. Lett. **83**, 5425 (2003).
[14] E. L. Ivchenko and G. Pikus, *Superlattices and Other Heterostructures* (Springer, New York, 1995).
[15] E. Blackwood, M. J. Snelling, R. T. Harley, S. R. Andrews, and C. T. B. Foxon, Phys. Rev. B **50**, 14 246 (1994).
[16] A. Siarkos, E. Runge, and R. Zimmermann, Phys. Rev. B **61**, 10 854 (2000).
[17] *Matlab v6.1* (The MathWorks Inc., Natick, 2001).
[18] M. Grochol, F. Grosse, and R. Zimmermann, J. Lumin. **112**, 208 (2005).
[19] H. Haug and S. W. Koch, *Quantum Theory of the Optical and Electronic Properties of Semiconductors* (World Scientific, Singapore, 1994).
[20] S. Glutsch, D. S. Chemla, and F. Bechstedt, Phys. Rev. B **54**, 11 592 (1996).
[21] W. H. Press, S. A. Teukolsky, W. T. Vetterling, and B. P. Flannery, *Numerical Recipes in C++* (Cambridge University Press, Cambridge, England, 2002).